Title

Xanthophyll-cycle based model of the rapid photoprotection of Nannochloropsis in response to regular and irregular light/dark sequences

Journal

The Journal of Chemical Physics, 156(20)

ISSN

0021-9606

Authors

Short, Audrey H

Fay, Thomas P

Crisanto, Thien

et al.

Publication Date

2022-05-28

DOI

10.1063/5.0089335

The Journal of Chemical Physics

Xanthophyll-cycle based model of the rapid photoprotection of *Nannochloropsis* in response to regular and irregular light/dark sequences

Cite as: J. Chem. Phys. **156**, 205102 (2022); https://doi.org/10.1063/5.0089335
Submitted: 24 February 2022 • Accepted: 05 May 2022 • Accepted Manuscript Online: 09 May 2022 • Published Online: 31 May 2022

Audrey H. Short, Thomas P. Fay, Thien Crisanto, et al.

The Journal of Chemical Physics ARTICLE scitation.org/journal/jcp

Xanthophyll-cycle based model of the rapid photoprotection of *Nannochloropsis* in response to regular and irregular light/dark sequences

Cite as: J. Chem. Phys. 156, 205102 (2022); doi: 10.1063/5.0089335
Submitted: 24 February 2022 • Accepted: 5 May 2022 •
Published Online: 31 May 2022

Audrey H. Short,[1,2,3] Thomas P. Fay,[4] Thien Crisanto,[2,5] Johanna Hall,[6] Collin J. Steen,[2,3,4] Krishna K. Niyogi,[2,5,7] David T. Limmer,[1,3,4,8,9] and Graham R. Fleming[1,2,3,4,a)]

AFFILIATIONS

[1] Graduate Group in Biophysics, University of California, Berkeley, California 94720, USA
[2] Molecular Biophysics and Integrated Bioimaging, Division Lawrence Berkeley National Laboratory, Berkeley, California 94720, USA
[3] Kavli Energy Nanoscience Institute, Berkeley, California 94720, USA
[4] Department of Chemistry, University of California, Berkeley, California 94720, USA
[5] Department of Plant and Microbial Biology, University of California, Berkeley, California 94720, USA
[6] Department of Environmental Engineering, Georgia Institute of Technology, Atlanta, Georgia 30332, USA
[7] Howard Hughes Medical Institute, University of California, Berkeley, California 94720, USA
[8] Chemical Science Division, Lawrence Berkeley National Laboratory, Berkeley, California 94720, USA
[9] Material Science Division, Lawrence Berkeley National Laboratory, Berkeley, California 94720, USA

Note: This paper is part of the JCP Special Topic on Photosynthetic Light-Harvesting and Energy Conversion.
[a)]**Author to whom correspondence should be addressed:** grfleming@lbl.gov

ABSTRACT

We explore the photoprotection dynamics of *Nannochloropsis oceanica* using time-correlated single photon counting under regular and irregular actinic light sequences. The varying light sequences mimic natural conditions, allowing us to probe the real-time response of non-photochemical quenching (NPQ) pathways. Durations of fluctuating light exposure during a fixed total experimental time and prior light exposure of the algae are both found to have a profound effect on NPQ. These observations are rationalized with a quantitative model based on the xanthophyll cycle and the protonation of LHCX1. The model is able to accurately describe the dynamics of non-photochemical quenching across a variety of light sequences. The combined model and observations suggest that the accumulation of a quenching complex, likely zeaxanthin bound to a protonated LHCX1, is responsible for the gradual rise in NPQ. Additionally, the model makes specific predictions for the light sequence dependence of xanthophyll concentrations that are in reasonable agreement with independent chromatography measurements taken during a specific light/dark sequence.

INTRODUCTION

Under ideal conditions of low light, photosynthesis is a highly efficient metabolic process.[1] When subjected to non-ideal environmental conditions such as high light (HL) exposure, most photosynthetic organisms rely on protective pathways to prevent damage that occurs when reactive oxygen species form.[2–4] Non-photochemical quenching (NPQ) pathways can quench excess energy and dissipate it as heat. However, since these protective pathways are not instantaneously activated or de-activated with changing light levels, organisms can be left under- or over-protected. Light levels can change rapidly over the course of a day, leading to inefficient energy use and damage.[5,6] Previous studies have shown that optimizing the photoprotective pathways used to combat excessive

light can increase an organism's biomass yields.[7,8] In addition, the suite of mechanisms used by plants and algae overlap in timescale and known biochemical components, making delineation of specific mechanisms difficult. Here, we study an organism with an apparently simpler, but substantial, response to a variety of light/dark exposures and build a model based on known biochemical actors with which to confront the data.

Interest in understanding the photoprotective pathways in *Nannochloropsis oceanica* is growing due to its high lipid production, which can be utilized in the biofuel industry.[9,10] *N. oceanica* has a high NPQ capacity, a comparatively simple pigment composition,[11,12] as well as a small diameter of ~3 μm, making it amenable to spectroscopy and, thus, a promising organism for mechanistic studies of NPQ pathways. *N. oceanica* contains only chlorophyll (Chl) *a* in its antenna, as well as the xanthophyll (VAZ) cycle pigments, violaxanthin (V), antheraxanthin (A), and zeaxanthin (Z), and the carotenoid vaucheriaxanthin.[13,14] It does not contain the carotenoid, lutein, that is commonly found in other algal and plant species, which enables more direct analysis of the carotenoids involved in quenching. The xanthophylls are interconverted via the VAZ cycle, which requires the enzymes violaxanthin de-epoxidase (VDE) and zeaxanthin epoxidase (ZEP), with A being an intermediate in the conversion of V to Z.[15] Triggering of the NPQ response in oxygenic photosynthetic organisms generally involves a ΔpH-sensing protein. In *N. oceanica*, this role is likely played by LHCX1.[14] Finally, *N. oceanica* does not exhibit pronounced state transitions, which are prominent in *C. reinhardtii*.[16–18] Because we are considering the short-time response, we have opted not to use conventional divisions into rapidly reversible (qE) or Z-dependent (qZ) processes and, instead, simply refer to NPQ. Longer timescale studies may need to delineate qE and qZ.[12] In our previous live-cell snapshot transient absorption spectroscopic studies of wild-type *N. oceanica* and two mutants lacking either VDE or LHCX1, we found a very small response to excess light if either VDE or LHCX1 was absent.[11] In addition, we found clear signals from both the Z S_1 state and the Z radical cation when NPQ was turned on, but no such signal in the VDE mutant nor the LHCX1 mutant even though it contained Z in high light. These observations suggest the importance of a joint action of LHCX1 and Z, with Z binding to a pigment–protein complex (putatively LHCX1) to create the quencher.

In this study, we explore NPQ in *N. oceanica* via fluorescence lifetime snapshot measurements under regular and irregular fluctuating light sequences and their description via a biochemically informed model based on the VAZ cycle and the protonation/deprotonation of a pH sensor. By changing the light intensity over one to several minutes, we aim to simulate the dynamic fluctuations experienced in natural environments. The model makes specific predictions for xanthophyll concentrations that are compared with some preliminary snapshot high-performance liquid chromatography (HPLC) measurements taken under identical conditions to the fluorescence lifetime snapshots.

EXPERIMENTAL SETUP

Algal growth conditions

Nannochloropsis oceanica CCMP1779[13] was obtained from the National Center for Marine Algae and Microbiota (https://ncma.bigelow.org/) and cultivated in F2N medium.[19] Liquid cultures were grown to 2–5 × 10^7 cells/ml in continuous light at a photon flux density of 60 μmol photons m^{-2} s^{-1} at 22 °C. We refer to these cells as LL-grown cells. For HL-grown cells, liquid cultures were transferred to HL for 24 h at 350 μmol photons m^{-2} s^{-1} at 22 °C.

Time-correlated single photon counting

Time-correlated single photon counting results in a histogram of Chl *a* fluorescence decay, which is then fit to a biexponential decay function yielding a lifetime (τ_{avg}). These fluorescence lifetimes were captured at 15 s intervals, resulting in snapshots of fluorescence trajectory that track the changes in the fluorescence lifetime as a function of HL exposure. The amplitude-weighted average lifetime of the Chl *a* fluorescence decay is converted into a unitless form, similar to that measured in the conventional pulse-amplitude modulation technique using the following equation: $NPQ_\tau(t) = \frac{\tau_{avg}(0)-\tau_{avg}(t)}{\tau_{avg}(t)}$,[20] where $\tau_{avg}(0)$ and $\tau_{avg}(t)$ are the average lifetimes in the dark and at any time point t during the HL exposure, respectively.

An ultrafast Ti:sapphire coherent Mira 900f oscillator was pumped using a diode laser (Coherent Verdi G10, 532 nm). The center wavelength of the oscillator was 808 nm with a full width at half maximum of 9 nm. After frequency doubling the wavelength to 404 nm with a β-barium borate crystal, the beam was split between a sync photodiode, which was used as a reference for snapshot measurements, and the sample. To control exposure of the sample to the actinic light, three synchronized shutters located in the laser path, the actinic light path, and the path between the sample and the microchannel plate-photomultiplier tube detector (Hamamatsu R3809U) were controlled by a LABVIEW software sequence. The detector was set to 680 nm to measure Chl *a* emission. During each snapshot, the laser and detection shutters were opened, allowing an excitation pulse with a power of 1.7 mW to saturate the reaction center for 1 s while the emission was recorded. During HL periods, samples were exposed to white light with an intensity of 885 μmol photons m^{-2} s^{-1} (Leica KL 1500 LCD, peak 648 nm, FWHM 220 nm) by opening the actinic light shutter.

1 ml of *N. oceanica* culture was pelleted for 10 min at room temperature at 14 000 revolutions per minute (RPM) flash frozen, thawed at room temperature, and broken using FastPrep-24 at 6.5 m/s for 60 s. The pellet was flash frozen and broken two more times. Chlorophyll was extracted from the broken cells using 1 ml of 80% acetone, and total chlorophyll in the culture was quantified according to Porra *et al.*[21] The culture was then concentrated to ~40 μg Chl ml^{-1} by centrifuging for 5 min at room temperature at 4000 RPM. Samples were then dark-acclimated for 30 min prior to the experiment and placed in the custom-built sample holder on a sample stage. The LABVIEW sequence was altered for each regular and irregular sequence run to control exposure to light fluctuations.

High-performance liquid chromatography

Aliquots of *N. oceanica* algae in F2N media were taken at various time points during several irregular and regular actinic light sequences. Samples were then flash frozen in liquid nitrogen. After thawing, the aliquots of the same time point were pooled by centrifuging for 5 min at 4 °C at 14 000 × RPM to reach a cell count

of ~45 × 10^6. The cells were washed twice with H_2O and pelleted at 14 000 × RPM for 5 min. Then, the cells were again flash frozen and thawed at room temperature followed by breaking the cells using FastPrep-24 (MP Biomedicals LLC) at 6.5 m/s for 60 s. The bead beating step was repeated once before adding 300 μl of 100% cold acetone. The samples were centrifuged for 10 min (14 000 × RPM, 4 °C), and the supernatant was filtered (0.2 μm nylon filter) into HPLC vials. The supernatant was separated on a Spherisorb S5 ODS1 4.6 × 250 mm^2 cartridge column (Waters, Milford, MA) at 30 °C. Analysis was completed using a modification of Garcıa-Plazaola and Becerril.[22] Pigments were extracted with a linear gradient from 14% solvent A (0.1M Tris–HCl pH 8.0 dd$H_2$0), 84% (v/v) solvent B (acetonitrile), 2.0% solvent C (methanol) for 15 min, to 68% solvent C and 32% solvent D (ethyl acetate) for 33 min, and then to 14% solvent A (0.1M Tris–HCl pH 8.0 ddH2O), 84% (v/v) solvent B (acetonitrile), 2.0% solvent C (methanol) for 19 min. The solvent flow rate was 1.2 ml min^{-1}. Pigments were detected by A445 with reference at 550 nm by a diode array detector. Standard curves were prepared from concentrated pigments. The HPLC peaks were normalized to the total Chl *a* concentration.

RESULTS

General kinetic features of *N. oceanica* photoprotective response

During the first HL exposure for the LL-grown cells, the photoprotective response as quantified by NPQ_τ has an exponential growth, which gradually slows with continued exposure to HL. The maximum NPQ_τ values for each successive HL period, separated by periods of darkness, trace out a sigmoidal curve. In the subsequent exposures to HL, the response to the transition from dark to light is immediate [Fig. 1(a)]. In the light to dark transition, the relaxation rate of NPQ_τ is also rapid. When the dark period is less than or equivalent to the duration of the initial HL period, the cells appear to retain a memory of the previous NPQ_τ activation level [Fig. 1(a)]. However, when the dark period increases, the subsequent HL exposure begins at a much lower NPQ_τ value than in the preceding period [Figs. 1(b) and 1(c)]. As a result, the photoprotective mechanism seems to reset, causing the NPQ_τ curve during the second HL exposure to increase exponentially rather than grow more gradually [Figs. 1(b) and 1(c)].

To understand what molecular actors might be involved in the photoprotective pathways of *N. oceanica*, we acquired data for the HL-grown cells using the same light/dark sequences. This results in an increased Z concentration, [Z]. In the LL-grown cells, when the initial HL exposure is less than 2 min, the response is minimal [Fig. 2(a)]. Yet, HL-grown cells show a strong and increased NPQ_τ response. The curvature also differs from convex in LL-grown cells to concave in HL-grown cells during the first HL period (Fig. 2). While the second HL period shown in Fig. 2(a) exhibits a sigmoidal growth for LL-grown cells, the HL-grown cells show an immediate, significant NPQ_τ response. Interestingly, the maximum NPQ_τ value reached in each HL exposure remains approximately the same for LL- and HL-grown cells. The relaxation dynamics in the dark are also consistent regardless of the [Z]. In the light to dark transition, the cells for both treatments respond very rapidly and relax at the same rate to approximately equal NPQ_τ values.

A xanthophyll cycle-based NPQ_τ model

In order to understand the origin of the timescales of the experimental NPQ_τ response in its complex form, we propose a kinetic model based on the xanthophyll cycle. Specifically, we sought to construct a minimal model constrained by known biochemical processes, which was consistent with four common kinetic effects observed across the varied light conditions studied. The general kinetic features revealed in Figs. 1 and 2 include the rapid decay of NPQ_τ on transition to the dark and the presence of a slow decay following longer HL exposures are similar between the two treatments of algae. After a period of HL exposure, the slow increase in the NPQ_τ over the course of subsequent light exposures and the short induction period for response to initial light exposure are also similar for both samples.

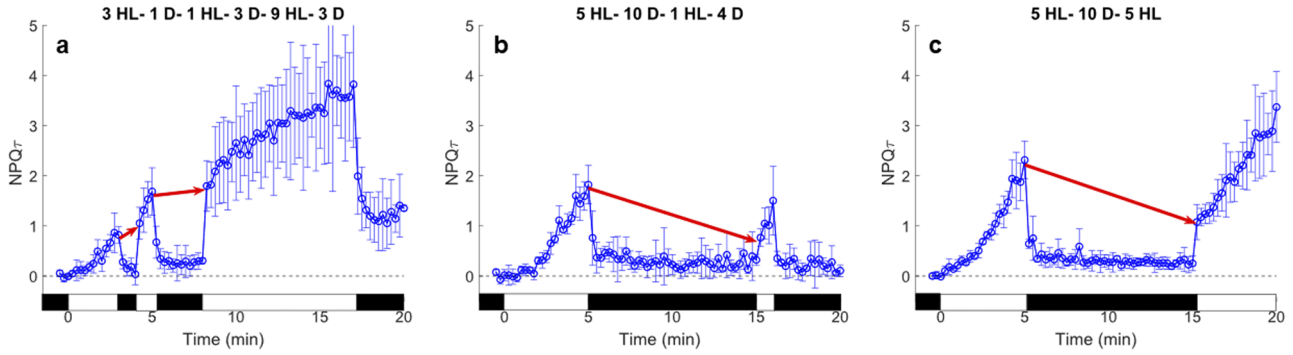

FIG. 1. Select irregular sequence NPQ_τ traces for LL-grown cells, which demonstrate that the cells' apparent memory is dependent on the duration of the dark period. (a) 3 min HL–1 min dark–1 min HL–3 min dark–9 min HL–3 min dark sequence demonstrates that when the dark relaxation period is shorter than the total prior HL exposure, the cells retain a memory of the proceeding NPQ_τ level before the light to dark transition. (b) 5 min HL–10 min dark–1 min HL–4 min dark and (c) 5 min HL–10 min dark–5 min HL show that when the dark period is longer than the HL period, the initial step in subsequent HL period is reduced. 95% confidence intervals are represented by error bars for n = 3. The red arrows connect the last HL point to the top of the initial response in the subsequent HL period. The black boxes at the bottom of each plot represent the dark periods, while the white boxes represent HL exposure.

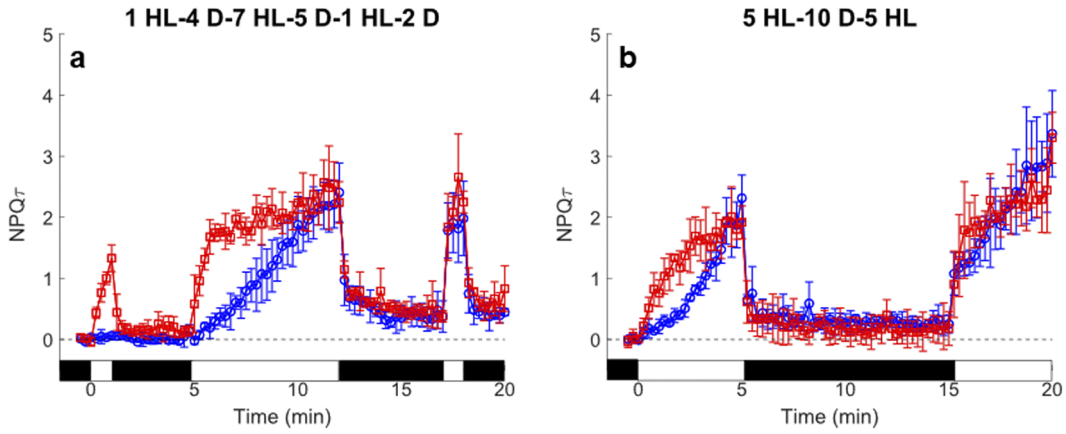

FIG. 2. HL-grown cells (red squares) compared to LL-grown cells (blue circles) for (a) 1 min HL–4 min dark–7 min HL–5 min dark–1 min HL–2 min dark and (b) 5 min HL–10 min dark–5 min HL dark sequences. The LL-grown cells exposed to the fluctuating light sequence in (a) show no significant response to the first HL stimulus. Conversely, HL-grown cells exhibit an immediate response. (b) The initial 5 min HL exposure results in different curvatures that are dependent on the pretreatment. HL-grown cells show an immediate, concave response to the first light period rather than a more gradual increase in NPQ_τ for LL-grown cells. In both (a) and (b), the maximum NPQ_τ values, as well as the extent and rate of recovery, are consistent between HL- and LL-grown cells. 95% confidence intervals are represented by error bars (n = 3). The black boxes at the bottom of each plot represent the dark periods, while the white boxes represent HL exposure.

First, the rapid decay and recovery of NPQ_τ to light after a period of HL exposure suggest that some quencher is produced in a primed state, which rapidly switches between an active and inactive form. The fast timescale is likely related to the lumen pH that is known to rapidly respond to light.[23] The "inactive" quencher must be relatively long lived in the dark phases for the NPQ_τ to retain a memory of previous light exposure. Second, the slow increase in the NPQ_τ over the course of light exposure suggests that the quencher must be formed during the light phases in a second light-dependent process. These observations could be explained by the formation of a Z-bound protein complex that acts as a quencher in response to a low lumen pH. Likely, the complex is between LHCX1 and Z given the known importance of both to NPQ in *Nannochloropsis*.[11] The formation of these quenchers is mediated by the xanthophyll cycle since we assume that LHCX1 also binds V. To de-epoxidize V to Z, any complexed V must first unbind from LHCX1. In the HL-grown algae, we expect a higher initial concentration of Z, which leads to a faster initial onset of quenching. Third, the minimal NPQ_τ response we see in LL-grown cells in 1 min of initial light exposure could be explained by a delay in the activation and deactivation of the conversion of V to Z. In our model, we account for this delay by including an activation step for the VDE enzyme, which mediates the V de-epoxidation. A response time in the light and dark phases of the conversion between the active and inactive forms on the order of 1 min would account for the induction time. Finally, the slow decay of the NPQ_τ during long dark phases suggests that we need to include the reverse step of the xanthophyll cycle, in which Z is epoxidized back to V by ZEP. This process would remove quenchers in the dark phases, which would account for the decrease in NPQ_τ after long dark phases.

Synthesizing these ingredients, we arrive at the following model, illustrated schematically in Fig. 3. Protein–violaxanthin (PV) complexes establish an equilibrium with dissociated V and protein (P). VDE in its active form (VDEa) irreversibly catalyzes the

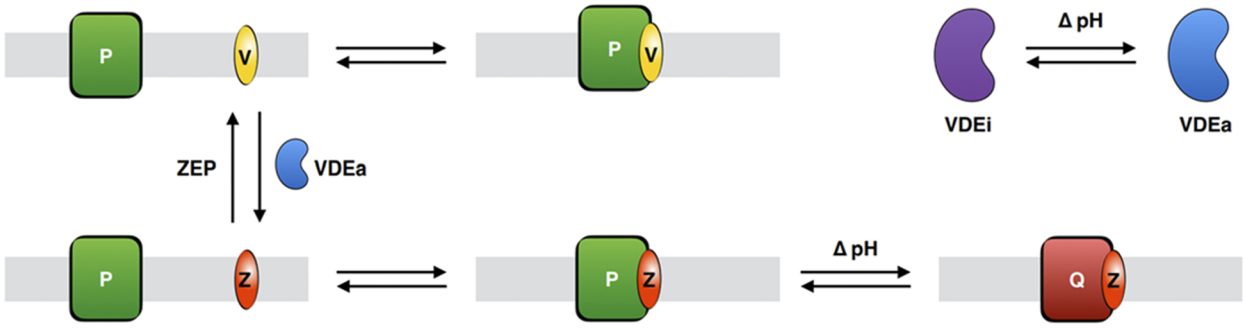

FIG. 3. Schematic of the model, showing the VAZ cycle and the involvement of VDE or ZEP (the intermediate step of A is omitted from the VAZ cycle for simplicity, and P is assumed to represent LHCX1, though the model does not require this). The activation of VDE and the conversion of PZ to Q occur in response to ΔpH.

de-epoxidation of V to Z. The activation of the de-epoxidation is mediated by light, due to changes in lumen pH. Z and unbound protein are in equilibrium with a protein–zeaxanthin (PZ) complex, the inactive quencher. Under HL conditions, this PZ complex converts to an active quencher Q in response to changes in ΔpH, and in darkness, it rapidly converts back to its inactive form. This likely reflects a protonation due to the altered lumen pH. To reduce the model complexity and the number of parameters needed, we have chosen to neglect the A intermediate in the xanthophyll cycle. These specific kinetic processes are

$$\mathrm{P} + \mathrm{V} \underset{k_{\mathrm{PV},b}}{\overset{k_{\mathrm{PV},f}}{\rightleftharpoons}} \mathrm{PV},$$

$$\mathrm{P} + \mathrm{Z} \underset{k_{\mathrm{PZ},b}}{\overset{k_{\mathrm{PZ},f}}{\rightleftharpoons}} \mathrm{PZ},$$

$$\mathrm{V} + \mathrm{VDEa} \xrightarrow{k_{\mathrm{V}}} \mathrm{Z} + \mathrm{ZDEa},$$

$$\mathrm{Z} \xrightarrow{k_{\mathrm{Z}}} \mathrm{V},$$

$$\mathrm{VDEi} \underset{k_{\mathrm{VDE},b}(I(t))}{\overset{k_{\mathrm{VDE},f}(I(t))}{\rightleftharpoons}} \mathrm{VDEa},$$

$$\mathrm{PZ} \underset{k_{\mathrm{Q},b}(I(t))}{\overset{k_{\mathrm{Q},f}(I(t))}{\rightleftharpoons}} \mathrm{Q},$$

where to obtain the model kinetic equations, we treat each step in the above scheme as an elementary process with rates defined by the arrows.

Our proposed model includes two light intensity, $I(t)$, dependent equilibria. Given that the lumen pH is known to respond on a much faster timescale than the kinetics that these experiments probe, we model the light intensity $I(t)$ dependent steps as instantaneously switching between a dark-phase value and a HL phase value,

$$k[I(t)] = \begin{cases} k_{\mathrm{dark}} & \text{if } I(t) = 0, \\ k_{\mathrm{light}} & \text{if } I(t) > 0, \end{cases} \tag{1}$$

for each light-dependent rate in the kinetic scheme. We assume that the system is initially in its dark-phase steady state, which leaves only three free concentrations, $[\mathrm{VDE}]_{\mathrm{tot}} = [\mathrm{VDEa}] + [\mathrm{VDEi}]$, $[\mathrm{X}]_{\mathrm{tot}} = [\mathrm{V}] + [\mathrm{Z}] + [\mathrm{PV}] + [\mathrm{PZ}] + [\mathrm{Q}]$, and $[\mathrm{P}]_{\mathrm{tot}} = [\mathrm{P}] + [\mathrm{PV}] + [\mathrm{PZ}] + [\mathrm{Q}]$. To obtain the NPQ_τ from this model, we assume that the fluorescence lifetime of chlorophyll *a* is given by

$$\frac{1}{\tau_F} = k_R + k_{NR} + k_Q[Q], \tag{2}$$

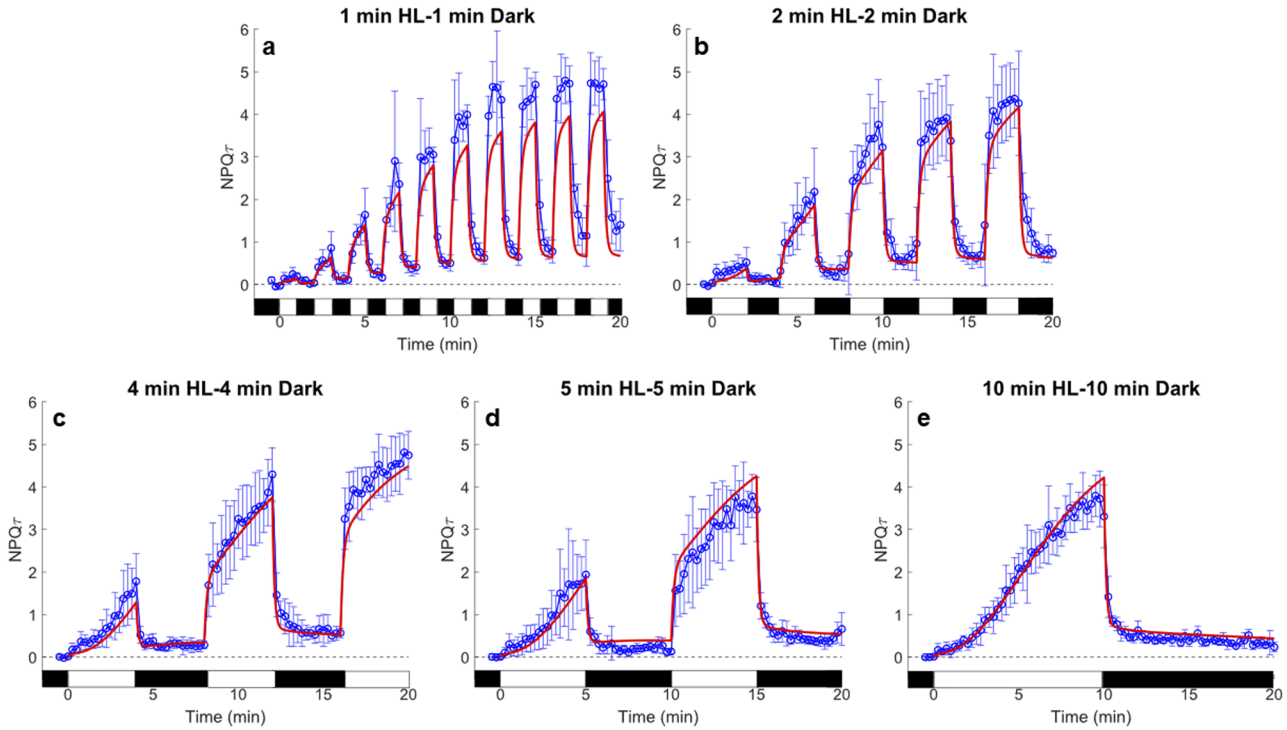

FIG. 4. NPQ_τ traces for each regular fluctuating light sequence for LL-grown cells. The model predicted NPQ_τ traces are shown as the red lines. Rapid fluctuating sequences, (a) and (b), show an increasing recovery baseline compared to slow fluctuating sequences (c)–(e), indicating that slower timescale NPQ components might not be able to relax in (a) and (b). Because of incomplete recovery in the 1 min HL–1 min dark sequence, this sequence was not included in the parameter fitting, which may be why the model underestimates NPQ_τ for this sequence. 95% confidence intervals are represented by error bars (n = 5). The black boxes at the bottom of each plot represent the dark periods, while the white boxes represent HL exposure.

where k_R is the radiative rate of Chl *a*, k_{NR} is the rate for de-excitation by other non-radiative processes, and k_Q is the quenching rate. With this, we model NPQ_τ as

$$NPQ_\tau = \tau_{F,0} k_Q [Q] - \tau_{F,0} k_Q [Q]_0, \tag{3}$$

where $\tau_{F,0}$ is the initial fluorescence lifetime and $[Q]_0$ is the initial concentration of the *Q* species.

To solve these kinetic equations numerically, we employ a system of dimensionless variables defined by $\widetilde{[A]} = \tau_{F,0} k_Q [A]$ to eliminate the k_Q parameter. In these reduced variables, the NPQ_τ signal is simply $NPQ_\tau = \widetilde{[Q]} - \widetilde{[Q]}_0$. In order to allow for consistent comparison between the parameters obtained in fitting the LL-grown algae datasets and HL-grown algae datasets, the NPQ_τ model value has to be scaled by the ratio of the fluorescence lifetimes under HL and LL conditions, which within the model is simply $1/\left(1 - \widetilde{[Q]}_0^{LL} + \widetilde{[Q]}_0\right)$, where $\widetilde{[Q]}_0^{LL}$ is the initial value $\widetilde{[Q]}$ obtained for the LL-grown dataset. Overall, then the HL-grown dataset NPQ_τ is given by

$$NPQ_\tau^{HL} = \frac{\tau_{F,0}^{HL}}{\tau_{F,0}^{LL}} \left(\widetilde{[Q]} - \widetilde{[Q]}_0\right) = \frac{\widetilde{[Q]} - \widetilde{[Q]}_0}{1 - \widetilde{[Q]}_0^{LL} + \widetilde{[Q]}_0}. \tag{4}$$

Furthermore, there is some parametric redundancy in fitting the model to the NPQ_τ data, because this signal depends only on $k_V[VDEa]$, so k_V can be scaled arbitrarily provided the total VDE concentration is scaled down by the same amount. In order to circumvent this problem, we fit the parameters $k_V[VDEa]^{eq}_{light}$ and $k_V[VDEa]^{eq}_{dark}$, and we only explicitly treat the relative activity of the VDE enzyme, $\alpha_{VDE} = [VDEa]/[VDEa]^{eq}_{light}$, as a kinetic variable. Here, $[VDEa]^{eq}_{light/dark}$ are the steady-state values of $[VDEa]$ in the light and dark phases of the experiment.

The remaining 15 model parameters were obtained by performing a least-squares fit to the experimental NPQ_τ data. Details are available in Appendix A. Due to variation between the experiments and shortcomings of the model, we could not find a parameter set that consistently captures the maximum NPQ_τ in both the periodic and irregular sequence datasets, so the model was fitted separately to these two datasets. Because longer timescale NPQ components were not included in the model, the 1-1 periodic sequence was found to heavily skew the model fitting with the periodic sequence data, so this was excluded in the fitting procedure. Additional simplified models were also tested in which various components of the current model were removed; for example, models in which VDE is assumed to respond instantaneously and models in which the Z to V conversion is neglected were tested. These simplified models did not adequately capture the NPQ_τ response to light fluctuations, and the model presented was found to be the minimal model that could describe the NPQ_τ responses. Further details of the model implementation, fitting, and error analysis are given in Appendix A.

NPQ response to regular and irregular light

When *N. oceanica* is exposed to periodic light fluctuations, the intensity of the response is dependent on time as well as the duration of the HL periodic exposure. The NPQ_τ data and model fits for the regular light fluctuations are presented in Fig. 4, and the model parameters are given in Tables I–III. The regular light fluctuations fall into two regimes, fast and slow, depending on the sequence duration. Sequences 1-1 and 2-2 [Figs. 4(a) and 4(b)] are considered to be fast fluctuations, while sequences 4-4, 5-5, and 10-10 [Figs. 4(c)–4(e)] have a qualitatively different appearance, and we term them slow fluctuations. The fast fluctuations have higher max NPQ_τ values of 4.73 and 4.34, respectively, which are caused by a raising baseline as

TABLE I. Fitted rate constants for the NPQ models for the LL period, LL irregular, and HL datasets. All model parameters refer to the reduced variable model, with parameters in min^{-1}.

Parameter	LL periodic	Error (2σ)	LL irregular	Error (2σ)	HL all sequences	Error (2σ)
$k_{PZ,f}$	5.86	2.5	6.28	2.6	3.91	1.5
$k_{PZ,b}$	0.325	7.2×10^{-2}	0.364	7.7×10^{-2}	0.861	0.23
$k_{PV,f}$	115	48	101	70	127	34
$k_{PV,b}$	5.09	1.0	6.00	3.4	5.72	0.68
$k_{Q,f,light}$	6.55	2.1	10.9	7.1	9.78	1.2
$k_{Q,b,light}$	2.14×10^{-2}	2.6×10^{-4}	1.51×10^{-2}	4.9×10^{-3}	2.00×10^{-3}	6.6×10^{-4}
$k_{Q,f,dark}$	1.60	3.5×10^{-3}	1.13	0.28	12.2	2.5
$k_{Q,b,dark}$	7.34	0.57	3.88	0.66	11.6	2.8
$k_{V,light}$ [a]	0.156	3.3×10^{-2}	0.158	7.0×10^{-2}	9.21×10^{-2}	1.2×10^{-2}
$k_{V,dark}$ [a]	1.13×10^{-3}	8.7×10^{-4}	4.53×10^{-4}	1.1×10^{-4}	1.30×10^{-3}	2.6×10^{-4}
$k_{Z,dark}$	5.29×10^{-2}	2.1×10^{-2}	6.21×10^{-2}	4.7×10^{-3}	1.10×10^{-3}	2.6×10^{-4}
$k_{VDE,light}$ [b]	3.84	1.6	1.84	0.72	3.58	1.1
$k_{VDE,dark}$ [b]	0.615	0.12	1.42	0.50	0.857	0.33

[a] $k_{V,light/dark} = k_V[VDEa]^{eq}_{light/dark}$ is the maximum rate of V to Z conversion in the light/dark phases.

[b] $k_{VDE} = k_{VDE,f} + k_{VDE,b}$ is the recovery rate for the VDE activation to its light/dark phase equilibrium value.

TABLE II. Equilibrium constants obtained for various equilibria in the model in reduced variables.

Parameter	LL periodic	Error (2σ)	LL irregular	Error (2σ)	HL all sequences	Error (2σ)
K_{PV}	22.7	9.5	16.8	10	22.3	4.0
K_{PZ}	18.1	9.5	17.3	8.0	4.54	1.6
$K_{X,dark}$[a]	2.13×10^{-2}	1.7×10^{-2}	7.29×10^{-3}	1.9×10^{-3}	1.25	0.36
$K_{X,light}$[a]	2.94	1.7	2.55	1.2	86.2	21
$K_{Q,dark}$	0.217	1.7×10^{-2}	0.292	3.7×10^{-2}	1.05	0.16
$K_{Q,light}$	306	99	721	350	4790	1600
$K_{PZ,eff,dark}$[b]	22.0	12	22.3	10	9.28	2.7
$K_{PZ,eff,light}$[b]	5550	2800	12 500	6900	21 700	12 000

[a] $K_X = [Z]_{eq}/[V]_{eq}$.
[b] $K_{PZ,eff} = ([PZ]_{eq} + [Q]_{eq})/[P]_{eq}[Z]_{eq}$.

TABLE III. Initial concentrations and the theoretical maximum NPQ_τ for the models fitted to the different datasets. All values are given for the reduced variable model, as described in the text, and as such all concentrations are unitless.

Parameter	LL periodic	Error (2σ)	LL irregular	Error (2σ)	HL all sequences	Error (2σ)
$[V]_0$	32.1	6.6	27.0	17	13.2	0.26
$[Z]_0$	0.684	0.55	0.197	0.14	16.5	4.8
$[PZ]_0$	8.60×10^{-2}	6.4×10^{-2}	2.88×10^{-2}	1.6×10^{-2}	1.78	0.61
$[Q]_0$	1.87×10^{-2}	1.4×10^{-2}	8.40×10^{-3}	4.7×10^{-3}	1.86	0.82
$[PV]_0$	5.06	0.40	3.85	0.10	6.99	2.2
$[P]_0$	6.96×10^{-3}	3.3×10^{-3}	8.46×10^{-3}	6.6×10^{-3}	2.38×10^{-2}	9.9×10^{-3}
$[X]_{tot}$	37.9	6.8	31.1	18	40.3	7.7
$[P]_{tot}$	5.17	0.41	3.90	0.10	10.6	3.6
NPQ_{max}	5.13	0.40	3.88	0.10	8.79	2.8

a result of incomplete relaxation of NPQ. Within the slow fluctuations, 5-5 and 10-10 have equivalent total HL exposure as the fast fluctuations, but do not exhibit a rising baseline, giving maximum NPQ_τ values that are lower at 3.76 and 3.79, respectively [Figs. 4(d) and 4(e)]. While the model succeeds in capturing the NPQ_τ values in HL periods for the slow fluctuations, it underestimates these values in the fast fluctuation, likely as a result of neglect of slower relaxation of long-timescale NPQ components.

The initial response to the first HL period clearly differs between the two fluctuation regimes. Examining the 10-10 sequence, the NPQ_τ curve has a sigmoidal shape with an inflection point at about 5 min, exhibiting an NPQ_τ value of 2. In sequences 4-4 and 5-5, the first HL period has a convex shape, which reaches an NPQ_τ value of ~2. However, the fast fluctuations have different initial responses to HL. In these cases, the initial photoprotective response is minimal. Several light/dark cycles must pass before the fast fluctuations exhibit rapid responses to the dark to light transition with concave curvature. When examining the HL period segments, they form a sigmoidal curve similar to the continuous HL curve in 10-10. Even with a variety of durations, the model correctly generates the convex curvature for the first HL period and the changes in the subsequent HL periods to a more gradual NPQ_τ increase.

In addition to the regular periodic sequences, irregular light fluctuations were also used (Fig. 5). Here, the limits of the model were probed by seemingly random light/dark durations, which more closely mimic random light changes in nature. Overall, the model was able to capture the immediate response the cells have in the light-to-dark and dark-to-light transitions as seen in both the regular and irregular sequences. The predicted NPQ_τ response also retains an apparent memory of HL when dark durations are less than the preceding HL exposure [Figs. 5(a)–5(f), 5(i), and 5(j)]. The same sigmoidal shape can be seen in both the model and experimental data for the HL periodic segments except in two sequences: 5-10-1-4 and 5-10-5 [Figs. 5(g) and 5(h)]. Particularly in the 5-10-1-4 sequence, the model overestimates the NPQ_τ response in the second HL exposure. A similar issue can be seen in Fig. 5(a) when the first HL period is 1 min, which does not elicit a response in LL-grown cells. The experimental data show the sigmoidal growth in maximum NPQ_τ in the second HL period, indicating that the quenching mechanism was not fully turned on during the first minute of HL.

In Fig. 6, we show the response and fits to irregular light/dark sequences for HL-grown algae. The difference in the initial response when the first light period is short [Figs. 6(a) and 6(b) vs Figs. 5(a) and 5(b)] is striking. In contrast, the rapid decrease in NPQ_τ on transition to the dark and the presence of a slow decay in NPQ_τ

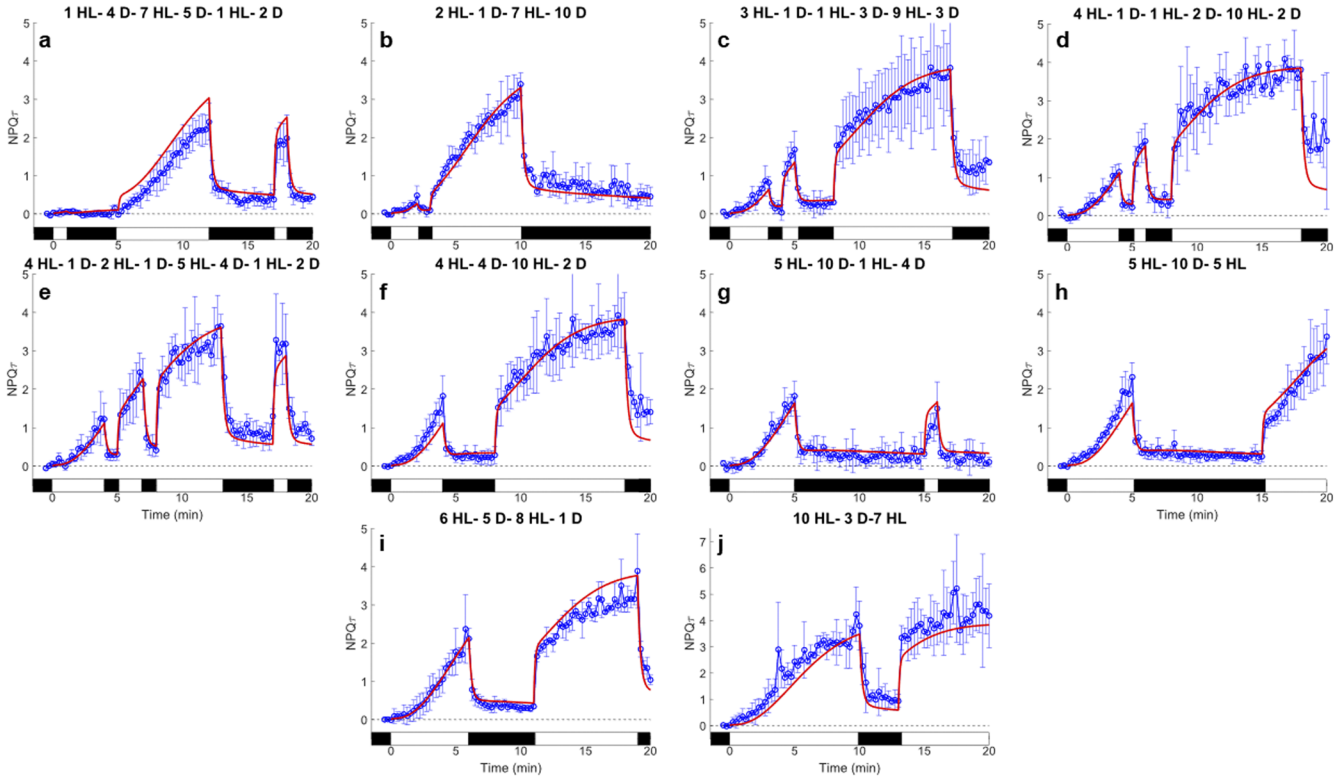

FIG. 5. NPQ_τ traces for irregular fluctuating light sequences of LL-grown cells. The model predicted NPQ_τ curve (red line) is also shown. The experimental NPQ_τ and predicted NPQ_τ curve for (a) 1 min HL–4 min dark–7 min HL–5 min dark–1 min HL–2 min dark, (b) 2 min HL–1 min dark–7 min HL–10 min dark, (c) 3 min HL–1 min dark–1 min HL–3 min dark–9 min HL–3 min dark, (d) 4 min HL–1 min dark–1 min HL–2 min dark–10 min HL–2 min dark, (e) 4 min HL–1 min dark–2 min HL–1 min dark–5 min HL–4 min dark–1 min HL–2 min dark, (f) 4 min HL–4 min dark–10 min HL–2 min dark, (g) 5 min HL–10 min dark–1 min HL–4 min dark, (h) 5 min HL–10 min dark–5 min HL, (i) 6 min HL–5 min dark–8 min HL–1 min dark, and (j) 10 min HL–3 min dark–7 min HL. As can be seen in (a), the model overestimates the slow, initial increase seen in the experimental data. The model similarly overshoots the secondary HL exposure in (g) after a 10 min dark period. Overall, the model is able to reproduce the rapid switch on/off with the transitions between light/dark and vice versa. 95% confidence intervals are represented by error bars (n = 3). The black boxes at the bottom of each plot represent the dark periods, while the white boxes represent HL exposure.

following longer HL exposures [e.g., Figs. 5(b) and 6(b)] are quite similar in two treatments. Clearly, at least some of the additional Z in the HL-grown cells is available for quenching on the 1 min timescale. Interestingly, maximum NPQ_τ values reached in both datasets are the same; they are clearly limited by something other than total [Z]. Overall, the model performs equally well for the two datasets.

In Tables I–III, we present the model parameters obtained from fitting the model to the experimental NPQ_τ datasets, all of which are given in the reduced units described above. The full set of rate constants in Table I, plus $[V]_0$ and $[P]_{tot}$, were fitted directly, which were then used to obtain the other parameters listed in Tables II and III. Model parameters for the two LL-grown datasets largely agree (to within two standard deviations), with the exception of $[P]_{tot}$, while there are more significant differences between the model parameters for the LL-grown and HL-grown algae, in particular, in the values of k_Z, k_V, $[X]_{tot}$, $[P]_{tot}$, and the other parameters that depend strongly on these. In the following two sections, we will highlight some of the points of interest regarding the model parameters and discuss what physical insight into xanthophyll-based NPQ can be gleaned from their values.

Origin of sigmoidal growth of NPQ_τ

One intriguing feature of the NPQ_τ signals is the remarkable difference in the responses of LL- and HL-grown algae. In the former case, a sigmoidal-like growth, $NPQ_\tau \propto 1/(ae^{-kt}+1)$, is observed, whereas in the latter case, a much simpler $NPQ_\tau \propto 1-e^{-kt}$ response is seen. In the former case, the growth rate of NPQ_τ increases then decreases, but in the latter case, the NPQ_τ growth rate is decreasing at all times during the light phases.

To explain this in qualitative terms, we note that there are two main factors that contribute to the growth of PZ and subsequently NPQ_τ. First, the availability of free P to which Z can bind, and second, the availability of Z. Assuming that V and P binding and unbinding are rapid, free P is created by the removal of V, pulling the PV binding equilibrium toward the unbound species. If there is a large excess of Z initially as in the HL-grown algae, then, free P is able to bind to Z as soon as it is produced, and no sigmoidal-like growth is observed. If there is a low initial concentration of Z as in the LL-grown algae, then P and Z build up significantly before

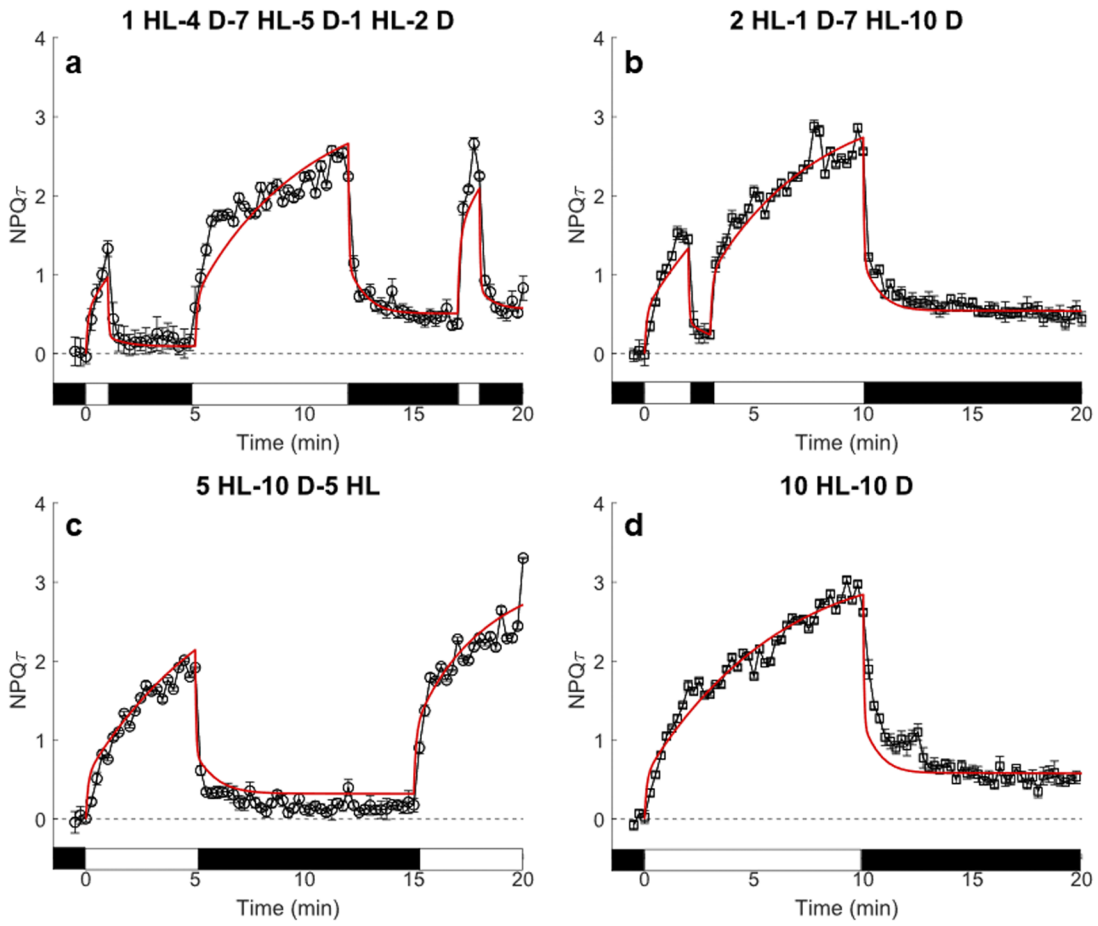

FIG. 6. Comparison of the model (red line) to the experimental data (black squares) for the HL-grown cells. This treatment causes the algal cells to accumulate a higher [Z]. The change in kinetics can be seen in the concave curves present in all the HL exposure periods during the experimental run. The experimental NPQ_τ and predicted NPQ_τ curve for HL-grown cells for sequences (a) 1 min HL–4 min dark–7 min HL–5 min dark–1 min HL–2 min dark, (b) 2 min HL–1 min dark–7 min HL–10 min dark, (c) 5 min HL–10 min dark–5 min HL, and (d) 10 min HL–10 min dark. The black boxes at the bottom of each plot represent the dark duration, while the white boxes represent HL exposure. 95% confidence intervals are represented by error bars (n = 3). The black boxes at the bottom of each plot represent the dark periods, while the white boxes represent HL exposure.

binding to form PZ, and the rate at which PZ is formed will, therefore, go through a maximum.

This is illustrated in Fig. 7, where we show the concentrations of Z, P, and PZ + Q for LL- and HL-grown models during 10 min of light exposure. In the LL-grown case, [P] passes through a maximum, and [Z] increases significantly, resulting in the total PZ concentration exhibiting sigmoidal-like growth. In the HL-grown case, however, the initial Z concentration is much larger, and as a result, neither Z nor P build up during the light exposure, so the total PZ concentration does not exhibit sigmoidal-like growth.

Under quasi-equilibrium assumptions, detailed in Appendix B, we find the following criterion for observing sigmoidal-like NPQ growth in our model,

$$\tau_V < \frac{K_{PV}[V]_0}{k_{PZ,f}[Z]_0}, \tag{5}$$

where $\tau_V^{-1} = k_V[\mathrm{VDEa}]^{eq}_{light}$ is the time-scale on which V is converted to Z in the light phases. When there is a large excess of V initially, as in the LL-grown algae, the right-hand side of Eq. (4) is large and the inequality is satisfied, and we observe sigmoidal growth. When more Z is present initially, as in the HL-grown algae, we do not see the sigmoidal-like growth.

Comparison of model concentration predictions to HPLC

The model produces the time-dependent xanthophyll concentrations, which can be independently compared with HPLC data for the various illumination sequences. Figure 8 compares experimental plots of normalized [Z](*t*) ([Z]/[V] + [A] + [Z]) with the model prediction for [Z](*t*) for the 5-10-5 sequence. The shape of the plot of the conventional[3] de-epoxidized quantity (([A]/2 + [Z])/[V] + [A]

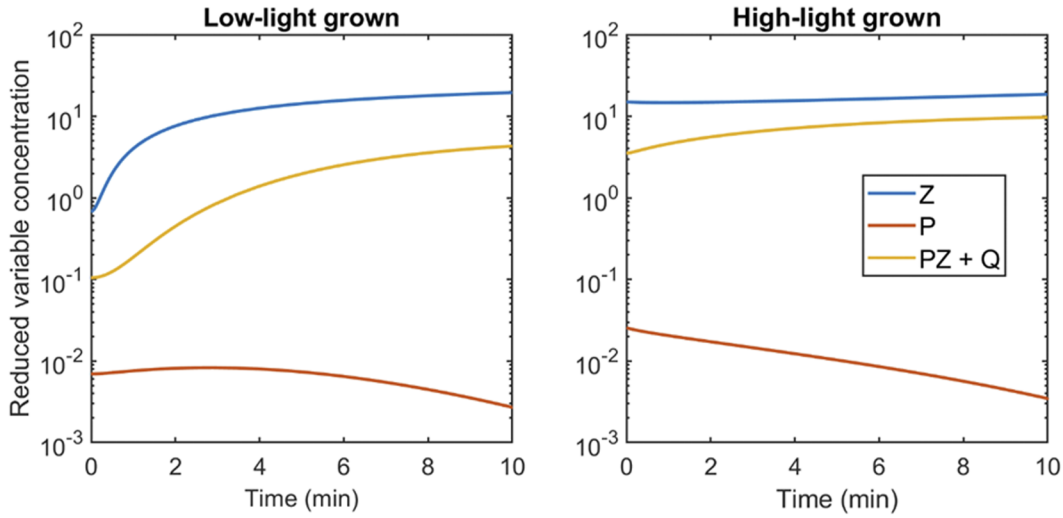

FIG. 7. Model predictions for the concentrations of Z, P, and PZ + Q for LL- and HL-grown algae during 10 min of light exposure.

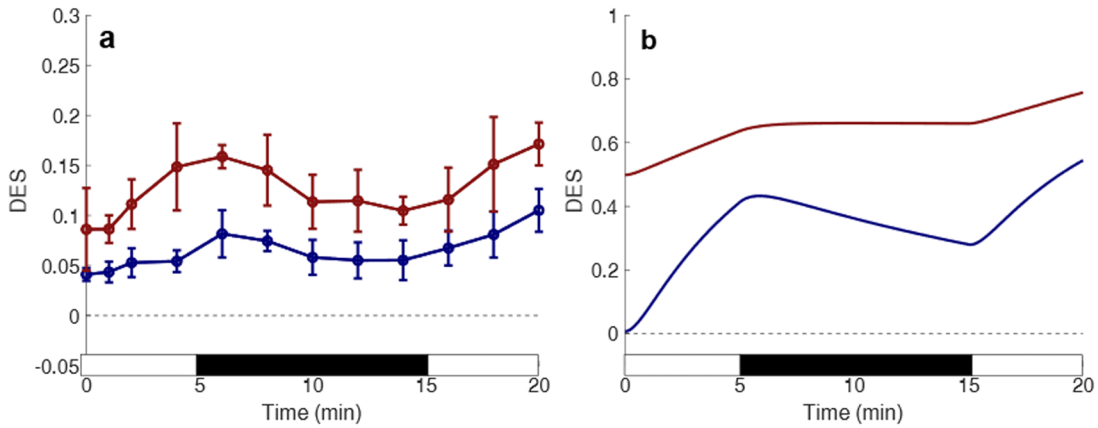

FIG. 8. De-epoxidation states (DES) taken at various timepoints throughout the 5 min HL–10 min dark–5 min HL sequence compared to the predicted DES. Results for HL-grown cells are shown in red, and the LL-grown results are depicted in blue. (a) The DES equation was modified to only include [Z] in the numerator since the model does not account for A contributing to the quenching state. (b) The model's predicted DES calculated using the predicted total [Z]/([V] + [Z]). 95% confidence intervals are represented by error bars (n = 3). The black boxes at the bottom of each plot represent the dark periods, while the white boxes represent HL exposure.

+ [Z]) is very similar for both HL-grown and LL-grown algae to those shown in Fig. 8(a).

One clear difference between the measurements and the model [Fig. 8(b)] is in the initial value of [Z]. However, in LL-grown algae, the NPQ_τ data strongly suggest that this pool of Z is not rapidly accessible to produce quenching in the first few minutes of HL exposure. If a constant [Z](0) is added to the model's LL prediction, the qualitative agreement with either model of de-epoxidized xanthophylls is good. In particular, the slow decrease in [Z] in the dark period is captured by the model, along with the steep increase in the second light period. However, we do not know when, or if, this initial pool of Z becomes active. We note that Jahns *et al.*[24] have shown that only a fraction of the total pool of V is accessible to VDE in plant thylakoid membranes even on a 120 min timescale as a result of V binding to specific light-harvesting proteins. In studies of understory leaves subject to rapid high intensity sun flecks, Adams *et al.* found that high levels of Z and A were maintained between sun flecks, even though the dissipation was minimal during the low light periods.[25] The degree to which the full [Z] is available for quenching complicates the comparison of the predicted and measured [Z(t)]. In the case of LL grown cells, equating the model [Z(t)] with ΔZ, i.e., subtracting the initial [Z] from the HPLC results, seems to be a reasonable approach because none of the initial [Z] is immediately available for NPQ (Fig. 2). For the HL-grown cells, however, at least some of the $[Z]_0$ is immediately available for NPQ, which suggests that this fraction may be free in the membrane rather than bound

to specific pigment–protein complexes. To quantify the initial [Z] availability, we plan in the future work to collect an extensive set of HPLC xanthophyll data for the light/dark sequences used in this work.

DISCUSSION

We now turn to the features of the model that underlie its description of the response of *N. oceanica* to excess light. We also comment on the numerical values of the fitting parameters and go on to explore whether the model can predict experimentally accessible quantities such as xanthophyll concentrations during our light/dark sequences.

The model correctly captures the change in NPQ response from accelerating (roughly exponential) to decelerating (roughly sigmoidal) with the crossover depending on the relative concentrations of V and Z, on a timescale dictated by the maximum de-epoxidation rate. The model allows us to ascertain timescales for the activation and deactivation of the quenching mechanism within the hypothetical LHCX1–Z complex. Under dark conditions, the deactivation rate ($k_{Q,f,\mathrm{dark}} + k_{Q,b,\mathrm{dark}}$) is found in the range 4–9 min^{-1}, which is very close to the light phase activation rate of the quenching ($k_{Q,f,\mathrm{light}} + k_{Q,b,\mathrm{light}}$), which is in the 7–11 min^{-1} range. The faster activation/de-activation timescale of PZ could reflect the time taken for protonation/deprotonation of LHCX1. However, given the relatively small variation between light and dark phases of the forward rate (roughly a 3–6 fold increase), where the lumen $[H^+]$ changes by much more, this seems unlikely. In our view, this rate reflects the timescale of a conformational change in the LHCX1 protein, which is triggered by a much more rapid protonation/deprotonation[23] or unbinding of LHCX1 from an antenna protein. A slower component of the NPQ$_\tau$ decay in the dark phases is likely due to the slower unbinding of Z from LHCX1 during the dark phases, the rate of which, $k_{PZ,b}$, is found to be roughly 0.5 min^{-1}.

Similarly, we find a rate for activation/deactivation of the VDE enzyme $k_{VDE} = k_{VDE,f} + k_{VDE,b}$ of 0.5–1.5 min^{-1} in the dark phases and 1.5–4 min^{-1} in the light phases. The relatively small variation between light and dark phases suggests that this does not directly reflect the protonation/deprotonation rate of VDE. Instead, this rate of activation could reflect a protonation-state dependent conformational change, or alternatively the rate at which the ascorbate substrate binds and unbinds from the enzyme, or unbinding VDE from the membrane.

The irregular sequence fits to LL-grown algae are used as a basis for fitting the HL-grown data. These fits captured the very different initial responses of HL- and LL-grown cells (Fig. 6). Comparing the HL fitted parameters to the LL fitted parameters, we find the most significant difference between the rate constants to be in the rates of de-epoxidation of V and epoxidation of Z (see Table I). The de-epoxidation rate k_V increases by a factor of ~3 in the dark phase and ~6 in the light phases between the HL- and LL-grown samples, while the epoxidation rate k_Z decreases by a factor of ~60 in the HL sample relative to the LL sample. These changes lead to the large observed difference in the initial Z concentration between the HL- and LL-grown samples, which leads to very different NPQ responses to fluctuating light. One possible explanation for these changes is different levels of expression of the VDE and ZEP enzymes when the algae are grown under HL and LL conditions.[26,27] HL and LL growth could also change the availability of other substrates involved in the (de-)epoxidation, as well as the average lumen pH and stroma pH, which are known to affect the activity of these enzymes.[28]

The other most significant differences between the HL- and LL-grown algae are the total concentrations of xanthophylls and LHCX1, with the xanthophyll pool being ~25% larger and the LHCX1 pool being around twice as large in the HL-grown algae.[12] Increasing the sizes of both pools increases the extent of quenching in the cells and the rate at which the quenching mechanism activates in response to HL. There are other small differences in the rate constants and equilibrium constants for the various processes between the HL- and LL-grown cells. These can likely be attributed to other changes between cells grown in different light conditions, for example, differences in the average dark and light phase lumen pH, and possible changes in the thylakoid membrane, stroma, and lumen compositions.[29] The maximum NPQ$_\tau$ values are the same in the HL- and LL-grown cells, though, which may indicate photoinhibition is occurring in HL-grown algae. However, measurements of periodic responses to different HL intensities and of gene expression levels under diverse illumination conditions should help in characterizing the origin of this rather surprising result.

The success in fitting the experimental data encouraged us to see if the model could predict quantities that could be subsequently measured. For example, the equilibrium constants listed in Table III can be related to binding free energies of various complexes and how they change under protonation. Our model also allows us to examine the relative binding constants for V and Z to the LHCX1 complex. For the Z binding, we must account for the two states of the PZ complex, so we compare K_{PV} with $K_{PZ,\mathrm{eff}} = (1 + K_Q)K_{PZ}$. Under dark conditions, the model predicts that V and Z bind similarly to the protein, with binding constants (in reduced units) of around 20. However, under HL conditions Z binds about 200–400 times more strongly than V to LHCX1. Temperature dependent studies should enable us to directly probe the binding free energies.

Model extensions

Although the simple xanthophyll cycle-based model of NPQ presented here provides a good foundation for understanding the kinetics of NPQ and its changes with fluctuating light, it still clearly has its limitations. For example, currently, the model cannot account for changes in light intensity beyond the simple binary fluctuations in light intensity. This could be accounted for by treating the light intensity-dependent rate constants phenomenological modeled, such as

$$k[I(t)] = \frac{k_{\mathrm{light}} - k_{\mathrm{dark}}}{1 + \left(\frac{I(t)}{I_{\mathrm{act}}}\right)^{-n}} + k_{\mathrm{dark}}, \tag{6}$$

which would reduce to Eq. (1) in the limit that n is large and the activation intensity I_{act} is similar to that used under the HL condition.

An alternative approach would be to incorporate this model with an extended model for the photosynthetic reaction network, which incorporates the variables that would directly affect the light-dependent rate constants, primarily the lumen pH. This approach could also allow the incorporation of feedback effects between the

quenching of chlorophyll excitations and the lumen pH (which affects the activation of quenching).

Another potential extension of the minimal model we have employed here is to incorporate more steps in the xanthophyll cycle and the quenching process itself. For example, our model makes no distinction between membrane-bound or protein-bound xanthophylls. This may be particularly important because ZEP is believed to reside in the stroma, whereas VDE is in the thylakoid lumen.[30]

Furthermore, in this model, we have excluded the A intermediate in the xanthophyll cycle, primarily to simplify the model and reduce the number of free parameters. A study by Arnoux *et al.* supports this decision as it indicates that V can be directly converted to Z without the A intermediate.[31] However, our preliminary HPLC results reveal that A is present in a significant amount. It may, therefore, be necessary to incorporate A and PA species into our current model to reconcile the differences between the theory and the experiment for the time dependence of Z concentration in HL-grown algae.

One aspect not explicitly included in our model is potential restructuring of the photosystem (PS) II light-harvesting complexes. State transitions (transfer of light-harvesting complexes from PSII to PSI) are not thought to occur in *N. oceanica*,[16] though they will likely contribute in other species.[18] Detachment of light-harvesting complexes from the PSII reaction center and subsequent quenching as a consequence of aggregation[32,33] may occur, but without time-dependent structural data at the membrane level, incorporation of such a phenomenon in a bottom-up model is not possible.

Additionally, the rapid regular sequences do not allow full recovery between HL periods, which do not fully recover during the dark periods. This led us to the possibility of longer timescale NPQ effects, which led us to fit the regular and irregular sequence data independently. The consistency of the best fit parameters (Tables I and II) within the error bounds, however, gives confidence in the overall self-consistency of the model. In developing and refining the model, we found that fitting the irregular sequence data provided a more rigorous test of the model than simply fitting the regular sequence data, due to the larger variability in NPQ response. We, therefore, suggest that irregular sequences of HL and dark or LL should be key measurements for organisms with more complex rapid photoprotection responses than *N. oceanica*.

CONCLUDING COMMENTS

The fits in Figs. 4–6 demonstrate that a model containing only the pH-dependent interconversion of V and Z via the actions of enzymes VDE and ZEP together with the formation of a quenching complex, Q, can quantitatively describe the rapid response of *N. oceanica* to various sequences of alternating HL illumination and dark. For the sake of specificity, we associate Q with Z bound to the protonated LHCX1 protein, although, our model does not require this. Thus, *N. oceanica* appears to have a particularly simple, rapid system to dissipate excess absorbed light. Our model may provide a starting point to understand the more complex responses of land plants with their additional dissipative pathways.

The hierarchy of timescales from seconds to minutes seen here will certainly be present in organisms with more complex, multi-component photoprotection responses, as these timescales relate to fundamental biochemical processes. In our previous analysis of regular periodic illumination of *A. thaliana* and a range of NPQ mutants, we used a purely mathematical model to fit the data and then drew mechanistic conclusions from the responses of the various mutants in comparison to the wild type.[34] In contrast, the model described here is bottom-up and, therefore, can make much more specific (and quantitative) predictions than our earlier work. Building on the works of Zaks *et al.*[35] and Bennett *et al.*,[36] it should be a possible, but complex, undertaking to build on the approach to create a bottom-up model for plant rapidly reversible photoprotection.

ACKNOWLEDGMENTS

The authors thank Setsuko Wakao for help in growing *N. oceanica* and Nina Maryn for help with HPLC measurements. This work was supported by the U.S. Department of Energy, Office of Science, Basic Energy Sciences, Chemical Sciences, Geosciences, and Biosciences Division under, Field Work Proposal No. 449B. J.H. was supported by the Science Undergraduate Laboratory Internship at Lawrence Berkeley National Laboratory, Berkeley. T.P.F. and D.T.L. were supported by the U.S. Department of Energy, Office of Science, Basic Energy Sciences, CPIMS Program Early Career Research Program, under Award No. DE-FOA0002019. K.K.N. is an investigator of the Howard Hughes Medical Institute.

AUTHOR DECLARATIONS

Conflict of Interest

The authors have no conflicts to disclose.

DATA AVAILABILITY

The data that support the findings of this study are openly available in Zenodo at http://doi.org/10.5281/zenodo.6456268.

APPENDIX A: FURTHER DETAILS OF MODEL SIMULATION AND FITTING

The model parameters, θ, are fitted by performing a least-squares fit to the experimental NPQ_τ data. The function that is minimized is the sum of square residuals for the different high-light/dark sequences S,

$$\delta^2(\theta) = \sum_{i=1}^{N_{\mathrm{data}}} \left(\mathrm{NPQ}_\tau^{\mathrm{exp}}(t_i, S_i) - \mathrm{NPQ}_\tau^{\mathrm{model}}(t_i, S_i, \theta)\right)^2.$$

The covariance matrix of the fitted parameters, from which uncertainties in various model parameters are derived, is obtained from the Jacobian matrix of the residuals,

$$J_{i,n} = \frac{\partial}{\partial \theta_n}\left(\mathrm{NPQ}_\tau^{\mathrm{exp}}(t_i, S_i) - \mathrm{NPQ}_\tau^{\mathrm{model}}(t_i, S_i, \theta)\right).$$

The covariance of any two functions of the parameters, f and g, can be approximated as

$$\sum\nolimits_{fg} \approx \frac{\delta^2(\theta)}{N_{\mathrm{data}} - N_\theta}(\nabla_\theta f)^{\mathrm{T}}[\mathbf{J}^{\mathrm{T}}\mathbf{J}]^{-1}(\nabla_\theta g),$$

where N_θ is the number of parameters in the model.

The model kinetic equations are solved using the ode23s solver in Matlab. The optimization is performed using Matlab's fmincon starting from ~300 randomly chosen initial guesses for the parameter set. The models with the lowest least squares fit value are then chosen as the final models for each dataset. The Jacobian is evaluated using a second order central finite difference scheme with a step size of $\delta\theta_n = 10^{-3}\theta_n$.

APPENDIX B: THE SIGMOIDAL GROWTH CRITERION

Here, we take a more mathematical approach to describe the sigmoidal-like growth. We note that the binding and unbinding of P and V occur very rapidly, which enables us to apply the quasi-equilibrium/pre-equilibrium approximation to this step. With this, we can obtain [P], as a function of the other concentrations,

$$[\mathrm{P}] = \frac{[\mathrm{PV}]}{K_{\mathrm{PV}}[\mathrm{V}]} = \frac{[\mathrm{P}]_{\mathrm{tot}} - [\mathrm{PZ}]_{\mathrm{tot}}}{K_{\mathrm{PV}}[\mathrm{V}] + 1}.$$

Assuming $K_{\mathrm{PV}}[\mathrm{P}] \ll 1$, neglecting the back reverse step on the xanthophyll cycle where Z is converted back to V, and assuming the VDE activity adjusts rapidly, we can also obtain [V] as $[\mathrm{V}] = [\mathrm{V}]_0 e^{-t/\tau_{\mathrm{V}}}$, where $\tau_{\mathrm{V}}^{-1} = k_{\mathrm{V}}[\mathrm{VDEa}]^{\mathrm{eq}}_{\mathrm{light}}$.

The kinetic equation for the total concentration of PZ, $[\mathrm{PZ}]_{\mathrm{tot}} = [\mathrm{Q}] + [\mathrm{PZ}]$, in which the rate of assuming the unbinding of Z from PZ is negligible, can then be obtained as

$$\frac{\mathrm{d}}{\mathrm{d}t}[\mathrm{PZ}]_{\mathrm{tot}} \approx \frac{k_{\mathrm{PZ},f}[\mathrm{Z}]}{K_{\mathrm{PV}}[\mathrm{V}]_0}\left(\frac{1}{e^{-t/\tau_{\mathrm{V}}} + (K_{\mathrm{PV}}[\mathrm{V}]_0)^{-1}}\right) \times ([\mathrm{P}]_{\mathrm{tot}} - [\mathrm{PZ}]_{\mathrm{tot}}).$$

We see that the growth rate of PZ, and thus the NPQ_τ, has a sigmoidal component within these approximations. If the sigmoidal growth time-scale, τ_{V}, is shorter than the timescale on which PZ initially grows, $\tau_{\mathrm{PZ},0} = K_{\mathrm{PV}}[\mathrm{V}]_0/k_{\mathrm{PZ},f}[\mathrm{Z}]_0$ (assuming $K_{\mathrm{PV}}[\mathrm{V}]_0 \gg 1$), then the total concentration of PZ initially grows at an increasing rate. This gives the criterion for sigmoidal-like growth given above.

In order to obtain the sigmoidal-like growth criterion more carefully, we first solve the above kinetic equation. This can be done by assuming $[\mathrm{Z}] \approx [\mathrm{Z}]_0$ and then re-writing the differential equation as

$$\frac{\mathrm{d}y}{\mathrm{d}t} = -\frac{ay}{be^{-t/\tau_{\mathrm{V}}} + 1},$$

with $y = [\mathrm{PZ}]_{\mathrm{tot}} - [\mathrm{P}]_{\mathrm{tot}}$, $a = k_{\mathrm{PZ},f}[\mathrm{Z}]_0$, and $b = K_{\mathrm{PV}}[\mathrm{V}]_0$. This can be solved to give

$$y = y_0\left(\frac{b+1}{b + e^{-t/\tau_{\mathrm{V}}}}\right)^{\tau_{\mathrm{V}a}}.$$

Sigmoidal-like growth will be observed when the derivative of this passes through a maximum at $t > 0$. The stationary point on this curve is found to be

$$t^* = \tau_{\mathrm{V}} \ln\left(\frac{b}{\tau_{\mathrm{V}} a}\right) = \tau_{\mathrm{V}} \ln\left(\frac{K_{\mathrm{PV}}[\mathrm{V}]_0}{\tau_{\mathrm{V}} k_{\mathrm{PZ},f}[\mathrm{Z}]_0}\right).$$

This time is positive, and a sigmoidal-like growth is observed when the inequality in Eq. (5) is satisfied. It should be noted that these approximations do not capture the true kinetics quantitatively, in particular, the approximation of constant [Z] is somewhat weak, but these approximations do give insight into the origin of the sigmoidal-like growth in NPQ.

APPENDIX C: XANTHOPHYLL CONCENTRATION FOR LOW LIGHT AND HIGH LIGHT CELLS FOR ONE FLUCTUATING LIGHT SEQUENCE

The concentration of V in LL-grown *N. oceanica* decreases throughout the first HL-period as it is converted into A and Z, which simultaneously increase in concentration. The [V] stabilizes during

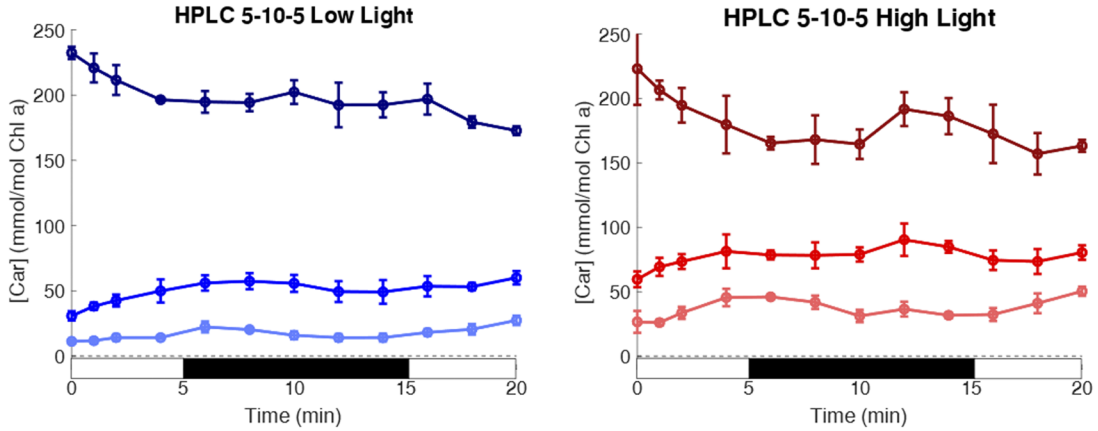

FIG. 9. Concentration of V, A, and Z for LL- (blue shades) and HL-grown (red shades) cells for 5-10-5 fluctuating light sequence. (Left) [V] (dark blue) decreases through the sequence, while [A] (blue) and [Z] (light blue) decrease and increase as a function of HL exposure. (Right) The trends for V, A, and Z are similar in HL-grown *N. oceanica*. [V] (dark red) is lower, while [A] (red) and [Z] (pink) are higher than the concentration in LL-grown plants. 95% confidence intervals are represented by error bars (n = 3). The black boxes at the bottom of each plot represent the dark periods, while the white boxes represent HL exposure.

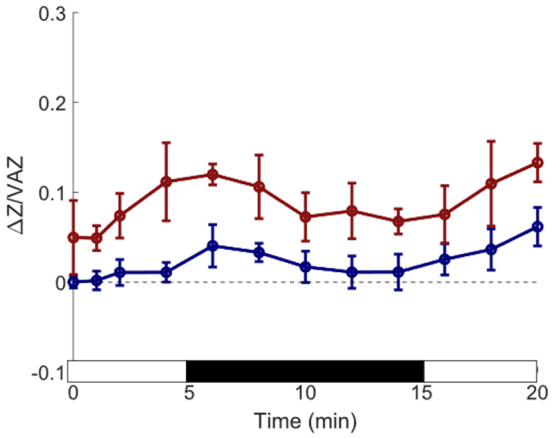

FIG. 10. ΔZ for LL-grown (blue) and HL-grown (red) normalized by the total VAZ concentration. The initial [Z], taken after 30 min of dark adaptation, was subtracted from LL-grown Z values. The initial [Z] for LL-grown cells was also subtracted from the HL-grown [Z].

the dark period while [Z] decreases more noticeably than [A]. In HL-grown cells, the [V] decreases more rapidly. The [A] and [Z] are also higher in HL-grown cells. Similar to the LL-grown cells, the [Z] is more responsive to the changes in illumination (Fig. 9).

As stated in the main text and shown in Fig. 10, while there is some amount of Z present before cells are exposed to HL in LL-grown cells, this is not readily available to contribute to quenching mechanisms. Since the model equates [Z(t)] with ΔZ, the initial [Z] available to incorporate was subtracted from [Z] in both the HL and LL-grown cells to produce ΔZ, which is normalized to the total VAZ value. The $[Z]_0$ in LL-grown cells was used to solve for the accessible Z as HL-grown cells have a higher initial [Z] and it appears that at least some are available for NPQ, suggesting that a fraction of Z is free in the membrane to rapidly interact with the quenching complex (Fig. 10).

REFERENCES

[1]R. E. Blankenship, *Molecular Mechanisms of Photosynthesis*, 3rd ed. (Wiley, 2021).
[2]M. Eskling, A. Emanuelsson, and H.-E. Åkerlund, "Enzymes and mechanisms for violaxanthin-zeaxanthin conversion," in *Regulation of Photosynthesis*, Advances in Photosynthesis and Respiration (Springer, Dordrecht, 2001), pp. 433–452.
[3]B. Demmig-Adams and W. W. Adams III, "Photoprotection and other responses of plants to high light stress," Annu. Rev. Plant Physiol. Plant Mol. Biol. **43**(1), 599–626 (1992).
[4]Z. Li, S. Wakao, B. B. Fischer, and K. K. Niyogi, "Sensing and responding to excess light," Annu. Rev. Plant Biol. **60**(1), 239–260 (2009).
[5]A. V. Ruban, "Crops on the fast track for light," Nature **541**(7635), 36–37 (2017).
[6]E. Kaiser, A. Morales, and J. Harbinson, "Fluctuating light takes crop photosynthesis on a rollercoaster ride," Plant Physiol. **176**(2), 977–989 (2018).
[7]C. Kulheim, J. Agren, and S. Jansson, "Rapid regulation of light harvesting and plant fitness in the field," Science **297**, 91 (2002).
[8]J. Kromdijk, K. Głowacka, L. Leonelli, S. T. Gabilly, M. Iwai, K. K. Niyogi, and S. P. Long, "Improving photosynthesis and crop productivity by accelerating recovery from photoprotection," Science **354**(6314), 857–861 (2016).
[9]Y. Ma, Z. Wang, C. Yu, Y. Yin, and G. Zhou, "Evaluation of the potential of 9 *Nannochloropsis* strains for biodiesel production," Bioresour. Technol. **167**, 503–509 (2014).
[10]L. Gouveia and A. C. Oliveira, "Microalgae as a raw material for biofuels production," J. Ind. Microbiol. Biotechnol. **36**(2), 269–274 (2009).
[11]S. Park, C. J. Steen, D. Lyska, A. L. Fischer, B. Endelman, M. Iwai, K. K. Niyogi, and G. R. Fleming, "Chlorophyll–carotenoid excitation energy transfer and charge transfer in *Nannochloropsis oceanica* for the regulation of photosynthesis," Proc. Natl. Acad. Sci. U. S. A. **116**(9), 3385–3390 (2019).
[12]V. U. Chukhutsina, R. Fristedt, T. Morosinotto, and R. Croce, "Photoprotection strategies of the alga *Nannochloropsis gaditana*," Biochim. Biophys. Acta, Bioenerg. **1858**(7), 544–552 (2017).
[13]A. Vieler, G. Wu, C.-H. Tsai, B. Bullard, A. J. Cornish, C. Harvey, I.-B. Reca, C. Thornburg, R. Achawanantakun, C. J. Buehl, M. S. Campbell, D. Cavalier, K. L. Childs, T. J. Clark, R. Deshpande, E. Erickson, A. Armenia Ferguson, W. Handee, Q. Kong, X. Li, B. Liu, S. Lundback, C. Peng, R. L. Roston, Sanjaya, J. P. Simpson, A. TerBush, J. Warakanont, S. Zäuner, E. M. Farre, E. L. Hegg, N. Jiang, M.-H. Kuo, Y. Lu, K. K. Niyogi, J. Ohlrogge, K. W. Osteryoung, Y. Shachar-Hill, B. B. Sears, Y. Sun, H. Takahashi, M. Yandell, S.-H. Shiu, and C. Benning, "Genome, functional gene annotation, and nuclear transformation of the heterokont oleaginous alga *Nannochloropsis oceanica* CCMP1779," PLoS Genet. **8**(11), e1003064 (2012).
[14]R. Litvín, D. Bína, M. Herbstová, and Z. Gardian, "Architecture of the light-harvesting apparatus of the eustigmatophyte alga *Nannochloropsis oceanica*," Photosynth. Res. **130**(1–3), 137–150 (2016).
[15]B. Demmig-Adams, J. J. Stewart, M. López-Pozo, S. K. Polutchko, and W. W. Adams, "Zeaxanthin, a molecule for photoprotection in many different environments," Molecules **25**(24), 5825 (2020).
[16]A. Alboresi, C. Le Quiniou, S. K. N. Yadav, M. Scholz, A. Meneghesso, C. Gerotto, D. Simionato, M. Hippler, E. J. Boekema, R. Croce, and T. Morosinotto, "Conservation of core complex subunits shaped the structure and function of photosystem I in the secondary endosymbiont alga *Nannochloropsis gaditana*," New Phytol. **213**(2), 714–726 (2017).
[17]C. Büchel, "Evolution and function of light harvesting proteins," J. Plant Physiol. **172**, 62–75 (2015).
[18]C. J. Steen, A. Burlacot, A. H. Short, K. K. Niyogi, and G. R. Fleming, "Interplay between LHCSR proteins and state transitions governs the NPQ response in intact cells of *Chlamydomonas* during light fluctuations," bioRxiv:2021.12.31.474662 (2022).
[19]O. Kilian, C. S. E. Benemann, K. K. Niyogi, and B. Vick, "High-efficiency homologous recombination in the oil-producing alga Nannochloropsis sp," Proc. Natl. Acad. Sci. U. S. A. **108**(52), 21265–21269 (2011).
[20]E. J. Sylak-Glassman, J. Zaks, K. Amarnath, M. Leuenberger, and G. R. Fleming, "Characterizing non-photochemical quenching in leaves through fluorescence lifetime snapshots," Photosynth. Res. **127**(1), 69–76 (2016).
[21]R. J. Porra, W. A. Thompson, and P. E. Kriedemann, "Determination of accurate extinction coefficients and simultaneous equations for assaying chlorophylls *a* and *b* extracted with four different solvents: Verification of the concentration of chlorophyll standards by atomic absorption spectroscopy," Biochim. Biophys. Acta, Bioenerg. **975**(3), 384–394 (1989).
[22]J. I. García-Plazaola and J. M. Becerril, "A rapid high-performance liquid chromatography method to measure lipophilic antioxidants in stressed plants: Simultaneous determination of carotenoids and tocopherols," Phytochem. Anal. **10**(6), 307–313 (1999).
[23]R. Zhang and T. D. Sharkey, "Photosynthetic electron transport and proton flux under moderate heat stress," Photosynth. Res. **100**(1), 29–43 (2009).
[24]P. Jahns, D. Latowski, and K. Strzalka, "Mechanism and regulation of the violaxanthin cycle: The role of antenna proteins and membrane lipids," Biochim. Biophys. Acta, Bioenerg. **1787**(1), 3–14 (2009).
[25]W. W. Adams III, B. Demmig-Adams, B. A. Logan, D. H. Barker, and C. B. Osmond, "Rapid changes in xanthophyll cycle-dependent energy dissipation and photosystem II efficiency in two vines, *Stephania japonica* and *Smilax australis*, growing in the understory of an open *Eucalyptus* forest," Plant, Cell Environ. **22**(2), 125–136 (1999).

[26]R. C. Bugos, S.-H. Chang, and H. Y. Yamamoto, "Developmental expression of violaxanthin de-epoxidase in leaves of tobacco growing under high and low light," Plant Physiol. **121**(1), 207–214 (1999).
[27]M. Eskling and H.-E. Åkerlund, "Changes in the quantities of violaxanthin de-epoxidase, xanthophylls and ascorbate in spinach upon shift from low to high light," Photosynth. Res. **57**(1), 41–50 (1998).
[28]C. E. Bratt, P.-O. Arvidsson, M. Carlsson, and H.-E. Åkerlund, "Regulation of violaxanthin de-epoxidase activity by pH and ascorbate concentration," Photosynth. Res. **45**(2), 169–175 (1995).
[29]A. Meneghesso, D. Simionato, C. Gerotto, N. La Rocca, G. Finazzi, and T. Morosinotto, "Photoacclimation of photosynthesis in the Eustigmatophycean *Nannochloropsis gaditana*," Photosynth. Res. **129**(3), 291–305 (2016).
[30]C. Reinhold, S. Niczyporuk, K. C. Beran, and P. Jahns, "Short-term down-regulation of zeaxanthin epoxidation in *Arabidopsis thaliana* in response to photo-oxidative stress conditions," Biochim. Biophys. Acta, Bioenerg. **1777**(5), 462–469 (2008).
[31]P. Arnoux, T. Morosinotto, G. Saga, R. Bassi, and D. Pignol, "A structural basis for the pH-dependent xanthophyll cycle in *Arabidopsis thaliana*," Plant Cell **21**(7), 2036–2044 (2009).
[32]A. V. Ruban and F. Saccon, "Chlorophyll *a* de-excitation pathways in the LHCII antenna," J. Chem. Phys. **156**(7), 070902 (2022).
[33]P. Horton, A. V. Ruban, and R. G. Walters, "Regulation of light harvesting in green plants (indication by nonphotochemical quenching of chlorophyll fluorescence)," Plant Physiol. **106**(2), 415–420 (1994).
[34]C. J. Steen, J. M. Morris, A. H. Short, K. K. Niyogi, and G. R. Fleming, "Complex roles of PsbS and xanthophylls in the regulation of nonphotochemical quenching in *Arabidopsis thaliana* under fluctuating light," J. Phys. Chem. B **124**(46), 10311–10325 (2020).
[35]J. Zaks, K. Amarnath, D. M. Kramer, K. K. Niyogi, and G. R. Fleming, "A kinetic model of rapidly reversible nonphotochemical quenching," Proc. Natl. Acad. Sci. U. S. A. **109**(39), 15757–15762 (2012).
[36]D. I. G. Bennett, G. R. Fleming, and K. Amarnath, "Energy-dependent quenching adjusts the excitation diffusion length to regulate photosynthetic light harvesting," Proc. Natl. Acad. Sci. U. S. A. **115**(41), 201806597 (2018).